

Search for heavy dark matter from dwarf spheroidal galaxies: leveraging cascades and subhalo models

Deheng Song^a Nagisa Hiroshima^{b,c,d} Kohta Murase^{e,f,g,a}

^aCenter for Gravitational Physics and Quantum Information, Yukawa Institute for Theoretical Physics, Kyoto University, Kyoto 606-8502, Japan

^bDepartment of Physics, Faculty of Engineering Science, Yokohama National University, Yokohama 240-8501, Japan

^cDepartment of Physics, University of Toyama, 3190 Gofuku, Toyama 930-8555, Japan

^dRIKEN Interdisciplinary Theoretical and Mathematical Sciences (iTHEMS), Wako, Saitama 351-0198, Japan

^eDepartment of Physics, The Pennsylvania State University, University Park, Pennsylvania 16802, USA

^fDepartment of Astronomy and Astrophysics, The Pennsylvania State University, University Park, Pennsylvania 16802, USA

^gCenter for Multimessenger Astrophysics, The Pennsylvania State University, University Park, Pennsylvania 16802, USA

E-mail: songdeheng@yukawa.kyoto-u.ac.jp, hiroshima-nagisa-hd@ynu.ac.jp, murase@psu.edu

Abstract. The *Fermi* Large Area Telescope (*Fermi*-LAT) has been widely used to search for Weakly Interacting Massive Particle (WIMP) dark matter signals due to its unparalleled sensitivity in the GeV energy band. The leading constraints for WIMP by *Fermi*-LAT are obtained from the analyses of dwarf spheroidal galaxies within the Local Group, which are compelling targets for dark matter searches due to their relatively low astrophysical backgrounds and high dark matter content. In the meantime, the search for heavy dark matter with masses above TeV remains a compelling and relatively unexplored frontier. In this study, we utilize 14-year *Fermi*-LAT data to search for dark matter annihilation and decay signals in 8 classical dwarf spheroidal galaxies within the Local Group. We consider secondary emission caused by electromagnetic cascades of prompt gamma rays and electrons/positrons from dark matter, which enables us to extend the search with *Fermi*-LAT to heavier dark matter cases. We also update the dark matter subhalo model with informative priors respecting the fact that they reside in subhalos of our Milky Way halo aiming to enhance the robustness of our results. We place constraints on dark matter annihilation cross section and decay lifetime for dark matter masses ranging from 10^3 GeV to 10^{11} GeV, where our limits are more stringent than those obtained by many other high-energy gamma-ray instruments.

Contents

1	Introduction	1
2	Subhalo model	2
3	Heavy dark matter model	4
4	Data analysis	7
5	Results and discussion	8
6	Summary	12
A	Spatial templates	15

1 Introduction

The nature of dark matter (DM) remains a mystery. Cosmological observations have shaped our understanding of the Universe, indicating that non-baryonic matter makes up approximately a quarter of the total energy density of the Universe [1, 2], thus giving rise to the DM problem. In the realm of particle physics, various candidates have been proposed to extend the Standard Model, and these candidates are currently under investigation through a combination of collider experiments, direct detection experiments, and astrophysical or cosmological observations (see Refs. [3–5] for recent reviews). For example, the Weakly Interacting Massive Particle (WIMP), which has long been a leading candidate, is already tightly constrained from multiple aspects for masses below approximately $m \lesssim \mathcal{O}(100)$ GeV [6, 7].

In this article, we focus on DM heavier than WIMPs, with masses above approximately 1 TeV. For such heavy DM, its relic abundance is not necessarily determined by thermal freeze-out [8–18]. In this case, collider experiments face kinematic limitations in creation processes, and the scattering rate with underground detectors decreases as the number density of incoming DM particles decreases. For this reason, high-energy astrophysical observation plays a crucial role because it provides a unique window for probing heavy DM. Many of current constraints on the annihilation cross sections and lifetime of heavy DM are based on observations of electromagnetic emission, which use various targets with distinct advantages to probe DM include the diffuse gamma-ray background [19–27], galaxy clusters [28–39], the Milky Way halo [40–47], and dwarf spheroidal galaxies (dSphs) [6, 48–62]. Multi-messenger approaches are also powerful, and other constraints on heavy DM include those from charged cosmic rays [63–71], neutrinos [33, 43, 59, 69, 72–74], and the cosmic microwave background (CMB) [75, 76]. Among these various indirect searches for heavy DM, dSphs are promising targets. The kinematics of stars in dSphs, which are satellite galaxies in subhalos of our Galaxy, indicate that they hold a huge amount of DM. However, the detailed DM density profile of each target is still uncertain and this dominates the uncertainty of the current limits for DM derived with dSphs. The nature of dSphs in subhalos that they have experienced tidal disruption under the potential of the Milky Way makes it difficult to obtain precise estimates.

One specific nature of heavy DM of $m_\chi \gtrsim \mathcal{O}(1)$ TeV is that the products from DM annihilation/decay, i.e. such as prompt gamma rays and electrons/positrons, interact with

background photon fields and magnetic fields before reaching Earth. Prompt emission, occurring on the scale of the DM mass, may cascade down to lower-energy levels through electromagnetic cascades (e.g., Refs. [20, 33]). In other words, heavy DM with much greater masses can still leave its signature in the energy range of GeV or even lower. Therefore, heavy DM can be probed by instruments like the *Fermi* Large Area Telescope (*Fermi*-LAT).

In this work, we investigate annihilation and decay signatures of heavy DM in 8 classical dSphs using 14-year *Fermi*-LAT data. These dSphs are nearby and their properties are relatively well probed. The secondary gamma-ray emission resulting from electromagnetic cascades of prompt gamma rays and electrons/positrons originating from heavy DM with masses exceeding 1 TeV are calculated based on Ref. [33] with the one-zone approximation. We incorporate the spatial extension of the target dSphs which retain the features of tidal interaction by constructing the emission template based on Ref. [77]. By performing the profile likelihood analysis, we constrain the annihilation cross section and decay lifetime of heavy DM.

The structure of the paper is as follows. In section 2, we describe the subhalo model for dSphs. In section 3, we explain the expected signals from heavy DM, including electromagnetic cascades in dSphs. We detail our data analysis in section 4. In section 5, we present and discuss our results, and we conclude the paper in section 6.

2 Subhalo model

The challenge of precisely modeling the DM density distribution in dSphs is well-recognized, and various models have been proposed in the literature (e.g. see Refs. [78–81]). In this work, we adopt the model proposed in Ref. [77] which applies informative prior respecting the fact that dSphs reside in subhalos of the Milky Way to improve the accuracy of parameter estimates for the DM density profile.

The DM density distribution is described using the Navarro-Frenk-White (NFW) profile [82] with truncation:

$$\rho_\chi(r) = \begin{cases} \rho_s \left(\frac{r}{r_s}\right)^{-1} \left(1 + \frac{r}{r_s}\right)^{-2}, & r < r_t, \\ 0, & r \geq r_t. \end{cases} \quad (2.1)$$

The profile is characterized by two parameters, ρ_s and r_s , for the NFW model and the truncation radius r_t . Likelihood analysis of stellar kinematics data results in degenerate constraints on the ρ_s - r_s plane. In this work, we consider the following 8 classical dSphs: Carina [83], Draco [84, 85], Fornax [83], Leo I [86], Leo II [87], Sculptor [83], Sextans [83], and Ursa Minor [85]. We exclude Sagittarius from our analysis, as observations indicate that this dSph is currently undergoing disruption [88], which could introduce significant uncertainty in the profile parameters. The distances and Galactic coordinates of these dSphs are listed in Table 1.

Since dSphs reside in subhalos of our Galaxy, they should experience tidal stripping by the Milky Way, leading to the current diversity in their DM density profiles. We take the Bayesian approach of Ref. [77] to reduce the uncertainties in the ρ_s , r_s , and r_t . The prior distribution suitable for each target dSph is generated using the model for subhalo evolutions [89]. The mass and the redshift distribution of accreting subhalos to the Milky Way is evaluated using the Extended Press-Schechter model [90]. The tidal mass-loss rate is evaluated at the pericenter of each accreted subhalo [91]. The evolution of the DM density profile

Name	Distance [kpc]	l [deg]	b [deg]
Carina	105.0 ± 6.0	260.11	-22.22
Draco	76.0 ± 6.0	86.37	34.72
Fornax	147.0 ± 12.0	237.10	-65.65
Leo I	254.0 ± 15.0	225.99	49.11
Leo II	233.0 ± 14.0	220.17	67.23
Sculptor	86.0 ± 6.0	287.54	-83.16
Sextans	86.0 ± 4.0	243.50	42.27
Ursa Minor	76.0 ± 3.0	104.97	44.80

Table 1. Distances and Galactic coordinates of 8 classical dSphs.

parameter is determined through the relationship derived in Ref. [92], which characterizes the evolution of the density profile parameters (ρ_s, r_s) as a function of the mass ratio before and after the tidal-mass loss. The parameter of the fitting function are calibrated against simulations. For the subhalo-satellite connection, we adopt the model of Ref. [93] with a threshold for the maximum circular velocity at accretion ($V_{\text{peak}} > 25$ km/s) and a velocity dispersion of $\sigma = 2.5$ km/s as specified in eq. 2 of Ref. [77]. These criteria are particularly suitable for classical dSphs [94].

We model the angular extension of the target dSphs by assuming the median values of ρ_s , r_s , and r_t obtained from the simulations. To further restrict the angular extension of the dSphs, we use the radii of the outermost stars [79] in the target dSphs. Specifically, we calculate the angular extension θ_Δ of each dSph up to

$$\theta_\Delta = \sin^{-1}(r_\Delta/d_c), \quad (2.2)$$

where d_c is the comoving distance of the dSph and

$$r_\Delta = \min(r_t, r_{\text{max}}). \quad (2.3)$$

The hierarchy between the estimated r_t and the observed radius of the outermost member star depends on the target dSph. So we introduce the quantity r_Δ for obtaining conservative J-factors. We calculate the J-factors of the dSphs for annihilation/decay ($J^{\text{ann}}/J^{\text{dec}}$) up to θ_Δ as follows,

$$J^{\text{ann}}(\theta_\Delta) = 2\pi \int_0^{\theta_\Delta} \sin \theta d\theta \int_{\text{l.o.s}} dl \rho_\chi^2(r; \rho_s, r_s), \quad (2.4)$$

and

$$J^{\text{dec}}(\theta_\Delta) = 2\pi \int_0^{\theta_\Delta} \sin \theta d\theta \int_{\text{l.o.s}} dl \rho_\chi(r; \rho_s, r_s). \quad (2.5)$$

In figure 1, the corner plot of ρ_s , r_s , and r_t parameters for Draco, obtained from the calculation based on the model proposed in Ref. [77], is shown as example. The figure presents the 2-dimensional density plots between every pair of parameters, accompanied by 1-dimensional histograms for each parameter. In the histograms, the median value and the 1-sigma percentile of the parameters are indicated by dashed vertical lines. Figure 2 shows the histograms for $J^{\text{ann}}(\theta_\Delta)$ (left panel) and $J^{\text{dec}}(\theta_\Delta)$ (right panel) of Draco, which are calculated based on the values of ρ_s , r_s , and θ_Δ obtained from the simulations. The median values of ρ_s , r_s , and r_t for the 8 target dSphs are listed in Table 2. Additionally, Table 2 provides r_{max} , θ_Δ , $J^{\text{ann}}(\theta_\Delta)$, and $J^{\text{dec}}(\theta_\Delta)$ for the target dSphs.

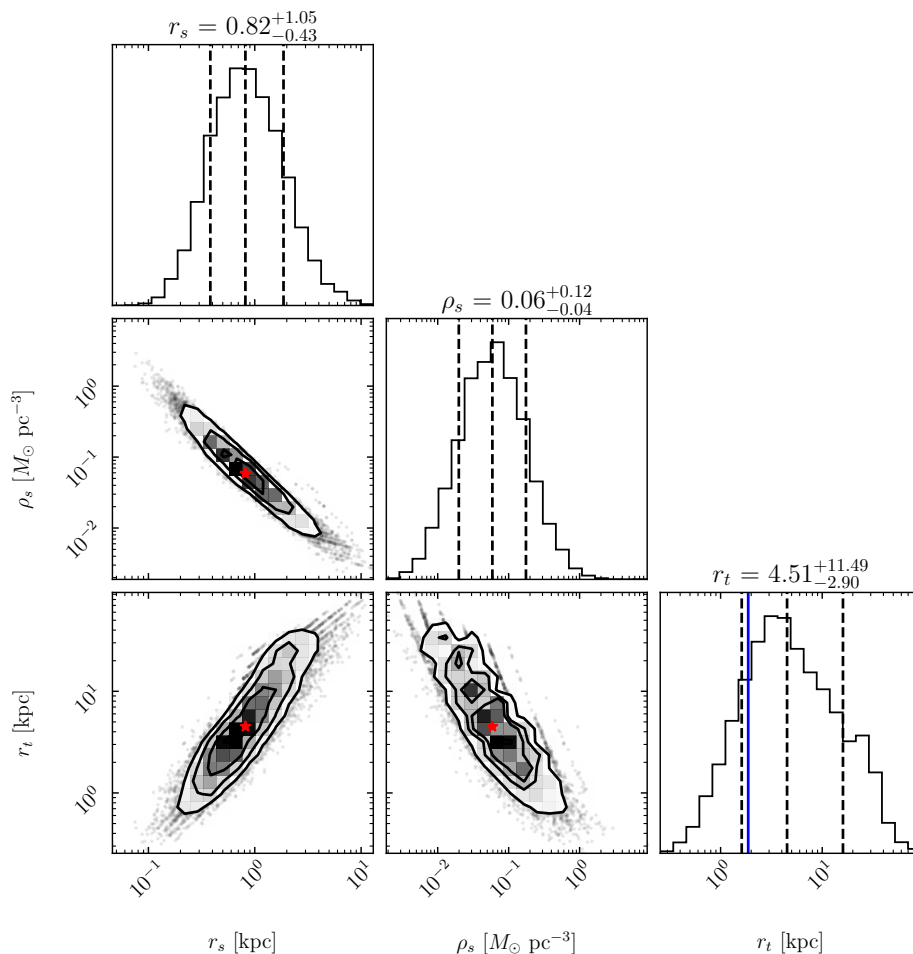


Figure 1. Corner plot [95] representing the distribution of ρ_s , r_s , and r_t for Draco, using the model proposed in Ref. [77]. In the histograms, the median value and the 1-sigma percentile of the parameters are indicated by dashed vertical lines. The red stars represent the median values of the parameters. Here r_{\max} of Draco is indicated by the blue solid line on the histogram of r_t .

3 Heavy dark matter model

We calculate the DM annihilation and decay spectra using `HDMspectra` [96]. Ref. [96] achieves the matching between the scale of the DM mass (up to the Planck scale) and that below the electroweak scale. Ref. [96] also includes hadronization calculation and matches with the `Pythia` [97]. In the scheme, the electroweak corrections are properly implemented. In this work, we consider DM masses m_χ ranging from 10^3 GeV to 10^{11} GeV. We assume the DM particles annihilate or decay into a pair of Standard Model particles with a 100% branching ratio. We consider 6 annihilation/decay channels: $b\bar{b}$, $\mu^+\mu^-$, $\tau^+\tau^-$, Z^0Z^0 , W^+W^- , and h^0h^0 .

The energy fluxes of generated gamma rays, $E_\gamma^2 \Phi_\gamma^{(\text{gen})}(E_\gamma, \theta_\Delta)$, from DM annihilation/decay processes in the dSphs are:

$$E_\gamma^2 \Phi_\gamma^{(\text{gen})}(E_\gamma, \theta_\Delta) = E_\gamma^2 \frac{dS_\gamma}{dE_\gamma} \times \begin{cases} \frac{\langle \sigma v \rangle}{8\pi m_\chi^2} \times J^{\text{ann}}(\theta_\Delta), & \text{for annihilation,} \\ \frac{1}{4\pi \tau_\chi m_\chi} \times J^{\text{dec}}(\theta_\Delta), & \text{for decay,} \end{cases} \quad (3.1)$$

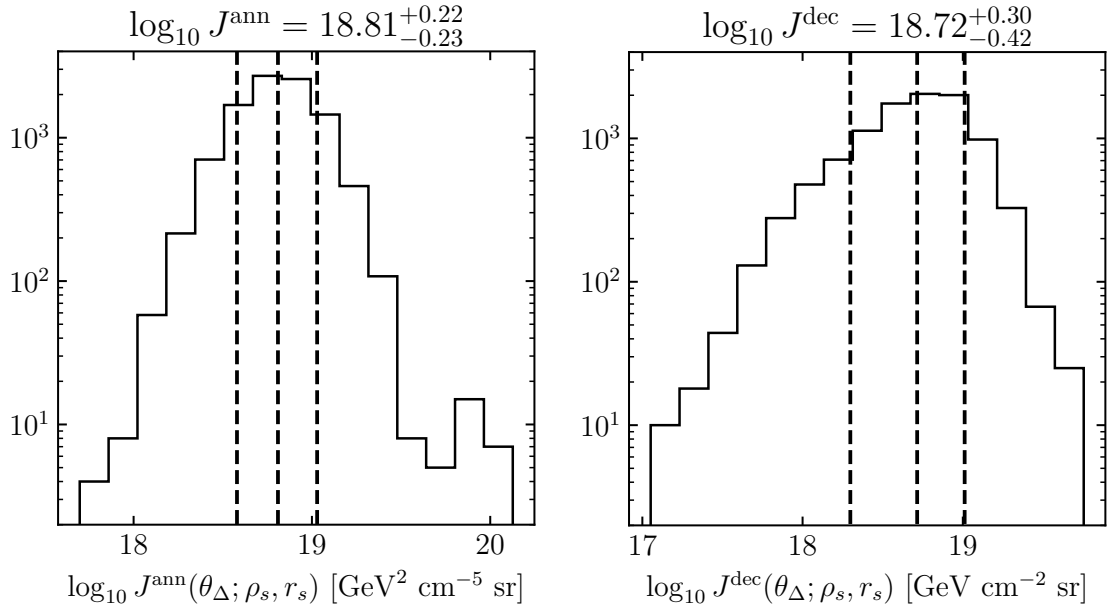


Figure 2. Histograms for $J^{\text{ann}}(\theta_{\Delta})$ and $J^{\text{dec}}(\theta_{\Delta})$ for Draco. In the histograms, the median value and the 1-sigma percentile of the parameters are indicated by dashed vertical lines.

Name	ρ_s [$M_{\odot} \text{ pc}^{-3}$]	r_s [kpc]	r_t [kpc]	r_{max} [kpc]	θ_{Δ} [deg]	$\log_{10} J^{\text{ann}}(\theta_{\Delta})$ [$\text{GeV}^2 \text{ cm}^{-5} \text{ sr}$]	$\log_{10} J^{\text{dec}}(\theta_{\Delta})$ [$\text{GeV cm}^{-2} \text{ sr}$]
Carina	$0.12^{+0.20}_{-0.08}$	$0.35^{+0.45}_{-0.17}$	$1.29^{+1.97}_{-0.68}$	$2.22^{+0.89}_{-0.44}$	0.70	$18.02^{+0.24}_{-0.26}$	$17.69^{+0.56}_{-0.48}$
Draco	$0.06^{+0.12}_{-0.04}$	$0.82^{+1.05}_{-0.43}$	$4.51^{+11.49}_{-2.90}$	$1.87^{+0.72}_{-0.32}$	1.41	$18.81^{+0.22}_{-0.23}$	$18.72^{+0.30}_{-0.42}$
Fornax	$0.05^{+0.08}_{-0.03}$	$0.96^{+0.85}_{-0.42}$	$5.82^{+9.57}_{-3.36}$	$6.27^{+2.62}_{-1.37}$	2.27	$18.23^{+0.17}_{-0.15}$	$18.46^{+0.31}_{-0.38}$
Leo I	$0.05^{+0.10}_{-0.03}$	$0.86^{+0.95}_{-0.44}$	$4.97^{+10.50}_{-3.06}$	$1.95^{+0.79}_{-0.41}$	0.44	$17.73^{+0.09}_{-0.08}$	$17.69^{+0.23}_{-0.31}$
Leo II	$0.06^{+0.15}_{-0.05}$	$0.62^{+0.98}_{-0.33}$	$2.86^{+7.03}_{-1.67}$	$0.82^{+0.35}_{-0.18}$	0.20	$17.56^{+0.10}_{-0.10}$	$17.22^{+0.22}_{-0.24}$
Sculptor	$0.06^{+0.11}_{-0.04}$	$0.80^{+1.00}_{-0.42}$	$4.32^{+10.75}_{-2.70}$	$2.67^{+1.10}_{-0.57}$	1.78	$18.65^{+0.19}_{-0.20}$	$18.67^{+0.33}_{-0.49}$
Sextans	$0.09^{+0.16}_{-0.06}$	$0.47^{+0.56}_{-0.22}$	$1.93^{+3.03}_{-1.05}$	$2.54^{+1.11}_{-0.59}$	1.28	$18.35^{+0.22}_{-0.25}$	$18.17^{+0.46}_{-0.47}$
Ursa Minor	$0.06^{+0.11}_{-0.04}$	$0.81^{+0.97}_{-0.42}$	$4.21^{+10.56}_{-2.58}$	$1.58^{+0.63}_{-0.31}$	1.19	$18.73^{+0.20}_{-0.20}$	$18.62^{+0.24}_{-0.34}$

Table 2. Halo properties of 8 classical dSphs based on the Bayesian analysis adopting prior distribution using the Extended Press-Schechter model [89].

where dS_{γ}/dE_{γ} is the gamma-ray spectra from DM annihilation/decay before accounting for electromagnetic cascades [20], $\langle\sigma v\rangle$ is the velocity-averaged cross section and τ_{χ} is the life time of the decaying DM. The redshift dependence does not appear because of the proximity of the dSphs.

The spectra of generated gamma rays should be modified through electromagnetic cascades. We follow Ref. [33] to calculate the cascade emission, approximating a galaxy to be a single zone. Details of electron-positron pair creation, synchrotron and inverse-Compton emission processes are considered. We solve the kinetic equation describing the evolution of

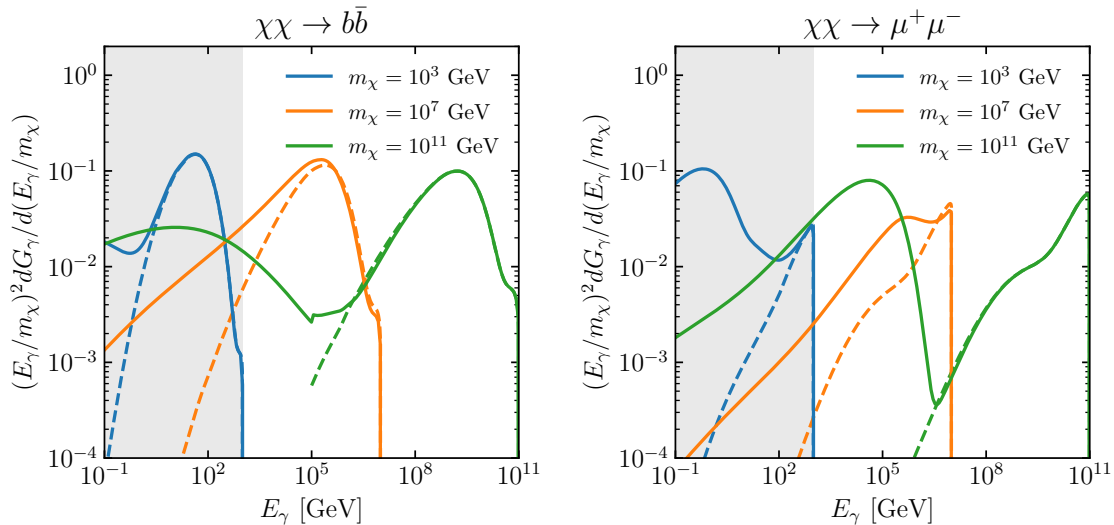


Figure 3. Gamma-ray spectra for annihilation of 3 DM masses: $m_\chi = 10^3$ GeV (blue), 10^7 GeV (orange), and 10^{11} GeV (green). Solid lines show the expected spectra at Earth with electromagnetic cascades considered, while dashed lines show the generated spectra before accounting for the electromagnetic cascades. The steep decline seen in the gamma-ray spectra corresponds to the kinematical cutoff by the DM mass. The gray bands indicate the energy range of the *Fermi*-LAT (100 MeV – 1 TeV).

the coupled system of photons and electrons [20, 33]. For the magnetic field in target dSphs, we assume $B = 1 \mu\text{G}$ as a fiducial value, while photons from the CMB [98] are taken as the background photon field for inverse-Compton emission. We also consider the infrared (IR) and optical radiation fields in dSphs, which are expected to be comparable to those in the clusters of galaxies [99, 100]. Therefore, as an approximation, we include the low-IR extragalactic background light model in Ref. [101] with 10 times enhancement to account for contributions from the stellar populations in the dSphs as in Refs. [33, 39]. We ignore the spatial diffusion because high-energy electrons/positrons lose their energies faster than they diffuse out in a galaxy. For the cascade calculation, we assume an escaping distance of the gamma rays at the r_{max} of the dSphs. This distance best represents the scale of the magnetic fields of the dSphs. As a result, the expected gamma-ray energy fluxes at Earth, $E_\gamma^2 \Phi_\gamma(E_\gamma, \theta_\Delta)$, from DM annihilation/decay processes in the dSphs are expressed as:

$$E_\gamma^2 \Phi_\gamma(E_\gamma, \theta_\Delta) = E_\gamma^2 \frac{dG_\gamma}{dE_\gamma} \times \begin{cases} \frac{\langle \sigma v \rangle}{8\pi m_\chi^2} \times J^{\text{ann}}(\theta_\Delta), & \text{for annihilation,} \\ \frac{1}{4\pi \tau_\chi m_\chi} \times J^{\text{dec}}(\theta_\Delta), & \text{for decay,} \end{cases}, \quad (3.2)$$

where dG_γ/dE_γ is the gamma-ray spectrum expected at Earth, which includes both attenuation and cascade components.

Figure 3 displays dG_γ/dE_γ (in solid lines) originating from DM annihilation using our benchmark parameters. The benchmark model assumes $B = 1 \mu\text{G}$. It also includes the CMB and the extragalactic background light with 10 times enhancement. We present the spectra for the $b\bar{b}$ channel in the left panel and the $\mu^+\mu^-$ channel in the right panel, considering three DM masses: $m_\chi = 10^3$ GeV, 10^7 GeV, and 10^{11} GeV (as shown respectively in blue, orange and green). The spectra are normalized for a single annihilation/decay event and are

shown in $(E_\gamma/m_\chi)^2 dG_\gamma/d(E_\gamma/m_\chi)$ so that they are approximately the same level. The total fluxes from the target dSphs are determined by eq. 3.2 and are suppressed when m_χ increases. The gray bands in figure 3 indicate the energy range of *Fermi*-LAT (100 MeV – 1 TeV). For heavy DM masses (e.g., $m_\chi = 10^7$ GeV and $m_\chi = 10^{11}$ GeV), the primary gamma-ray signals (which peak around m_χ) are beyond the reach of *Fermi*-LAT. However, secondary emission extends to lower energies and still have sizable contributions to the *Fermi* energy range. In figure 3, we also use dashed lines to show the generated spectra before accounting for the electromagnetic cascades.

4 Data analysis

We use the public software `fermipy` [102] to select the *Fermi*-LAT data, generate model templates convolved with the instrument response function, and perform the likelihood analysis. We select `P8R3_SOURCE` events (with both `FRONT` and `BACK` types) in 14-year *Fermi*-LAT data (from Aug 4 2008 to Aug 4 2022) with energies from 100 MeV to 1 TeV. This event class provides an intermediate photon selection and is most suitable for moderately extended sources. We apply the standard quality filter `DATAQUAL>0&&LATCONFIG==1` and limit the maximum zenith angle to 90° . For each dSph, the region of interest (ROI) is a $10^\circ \times 10^\circ$ square centering the dSph. The data are binned into $0.1^\circ \times 0.1^\circ$ pixels and logarithmic energy bins with 5 bins per decade.

The expected photon count u_{ij}^k from the i -th pixel and j -th energy bin in the k -th dSph is

$$u_{ij}^k = s_{ij}^k(A|m_\chi) + b_{ij}^k(\boldsymbol{\lambda}), \quad (4.1)$$

where s_{ij}^k and b_{ij}^k are respectively the signal and the background counts from the i -th pixel and j -th energy bin in the k -th dSph. The signal s_{ij}^k is determined by the DM model under consideration (including the subhalo model and electromagnetic cascades, see section 2 and 3) and depends on the amplitude parameter A (which is $\langle\sigma v\rangle$ for annihilation and $1/\tau_\chi$ for decay) for given m_χ . We generate the DM spatial templates using the `CLUMPY` package [103–105], assuming the Navarro-Frenk-White profile [82] with truncation. See Appendix A for the details of the DM halo templates before they are convolved with the *Fermi*-LAT Point Spread Function (PSF). The background b_{ij}^k includes all astrophysical emissions in the ROI and $\boldsymbol{\lambda}$ are the nuisance parameters for the background model. For the background components, we consider the Galactic diffuse emission¹, the isotropic diffuse emission², and the resolved point sources in the 4FGL-DR4 catalog. The nuisance parameters include the normalization and spectral parameters of the Galactic and isotropic diffuse emissions and the point sources within 5° from the dSphs. We also include point sources within a $20^\circ \times 20^\circ$ region centering the target dSph with their parameters fixed to the 4FGL values.

We adopt a joint Poisson likelihood function over all pixel i and energy bin j for the k -th dSph, which is

$$\mathcal{L}^k(\boldsymbol{\theta}) = \prod_i \prod_j \frac{\mu_{ij}^k(\boldsymbol{\theta})^{n_{ij}^k} e^{-\mu_{ij}^k(\boldsymbol{\theta})}}{n_{ij}^k!}. \quad (4.2)$$

Here, n_{ij}^k and $\mu_{ij}^k(\boldsymbol{\theta})$ are the observed and predicted photon counts at pixel i and energy bin j for the k -th dSph, respectively. In the meanwhile, $\boldsymbol{\theta} = \{A, \boldsymbol{\lambda}\}$ combine the DM and nuisance parameters.

¹`gll_iem_v07.fits`

²`iso_P8R3_SOURCE_V3_v1.txt`

We use profile likelihood method [106] to derive constraints on A . The test statistics (TS) for any A is defined as

$$\text{TS}(A) = -2 \log \left(\frac{\mathcal{L}(A, \hat{\boldsymbol{\lambda}})}{\mathcal{L}(\hat{\boldsymbol{\theta}})} \right), \quad (4.3)$$

where $\hat{\boldsymbol{\theta}}$ are the best-fitting parameters that maximize the likelihood function and $\hat{\boldsymbol{\lambda}}$ are the nuisance parameters that maximize the likelihood function for given A . The likelihood function $\mathcal{L}(\boldsymbol{\theta})$ can be the likelihood function $\mathcal{L}^k(\boldsymbol{\theta})$ of the k -th dSph when we put constraints from individual dSphs. Otherwise, we can use the total likelihood function of 8 dSphs, which is

$$\mathcal{L}^{\text{total}}(\boldsymbol{\theta}) = \prod_k \mathcal{L}^k(\boldsymbol{\theta}), \quad (4.4)$$

to put constraints on A from stacking 8 dSphs. In either case, the 95% confidence level (CL) limit on A is set by finding a $\text{TS} = 2.71$.

5 Results and discussion

In figure 4, we present the 95% CL upper limits on heavy DM annihilation cross section ($\langle\sigma v\rangle$) from Draco for the $b\bar{b}$ (left panel) and $\mu^+\mu^-$ (right panel) channels. We consider two scenarios: constraints derived with (solid blue lines) and without (dashed blue lines) electromagnetic cascades. Without cascades, constraints for $m_\chi \gtrsim 10^8$ GeV with *Fermi*-LAT data are weaker than those in the literature [107–109]. The constraints are improved with *Fermi*-LAT by taking the cascade into consideration and in this work, we derive novel constraints for m_χ up to 10^{11} GeV. For the $b\bar{b}$ channel, constraints with and without electromagnetic cascades are nearly identical at $m_\chi \sim 10^3$ GeV, indicating that the constraints are primarily determined by the prompt gamma-ray emission around the WIMP mass scale. Constraints with cascades become stronger than those without cascades as m_χ increases because electromagnetic cascades dominate the signal in the *Fermi*-LAT energy range. In the case of the $\mu^+\mu^-$ channel, the annihilation is dominantly leptonic, and prompt gamma rays arise from final-state radiation. Therefore, the constraints get tighter by almost two orders of magnitude at $m_\chi \gtrsim 10^3$ GeV by analyzing with the cascade contribution. Overall, the constraints on the annihilation cross section $\langle\sigma v\rangle$ decrease as m_χ increases, as the annihilation rate is proportional to $1/m_\chi^2$. The feature at $m_\chi \sim 10^7 - 10^9$ GeV originates from the transition of the dominant processes of the secondary emission in the energy range of this analysis, from an inverse-Compton emission-dominated region to a synchrotron emission-dominated region. This change is more significant for the $\mu^+\mu^-$ channel (again due to its being dominantly leptonic), leading to a peak in the constraints around 10^9 GeV. In figure 4, we also show limits with VERITAS [107] (dash dotted lines), MAGIC [108] (dotted lines) and HAWC [109] (dashed lines) constraints on the same dSph for comparison. To make the comparisons consistent, we rescale their constraints based on the J-factor used in this work, as listed in Table 2. We acknowledge that the linear scaling of the constraints ignores the discrepancies in the DM density profiles and PSFs of different instruments. Nonetheless, we anticipate these effects to be minor. Our constraints with cascades are notably stronger than the constraints from those high-energy instruments in both channels. However, without cascades, our results are suppressed by VERITAS and MAGIC for $m_\chi \gtrsim 10^4$ GeV. In figure 4, we also show the thermal

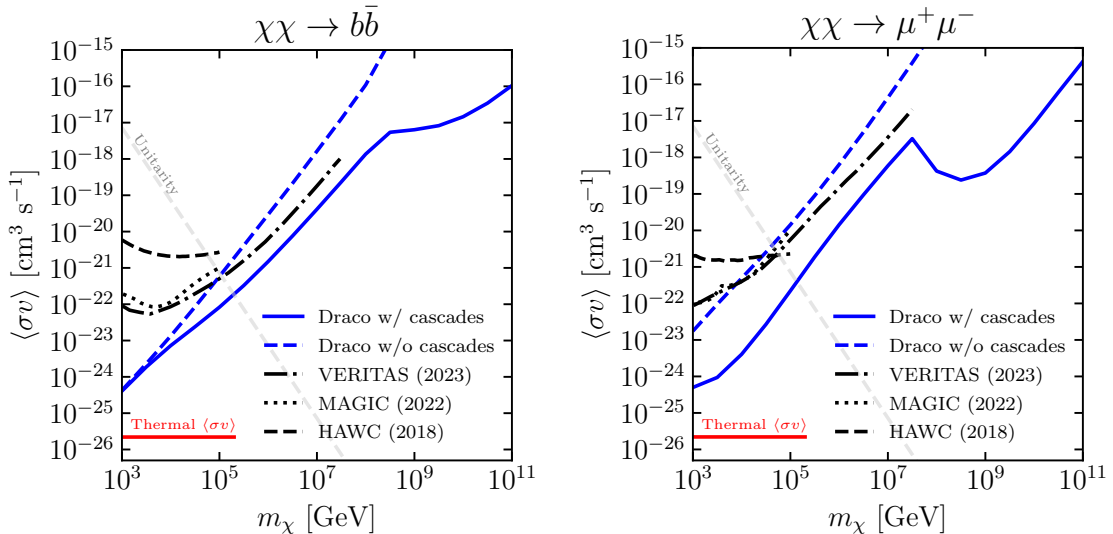


Figure 4. 95% CL upper limits on the annihilation cross section $\langle\sigma v\rangle$ for the $b\bar{b}$ (left panel) and $\mu^+\mu^-$ (right panel) channel from Draco. Constraints with (solid blue lines) and without (dashed blue lines) electromagnetic cascades are included. The constraints are compared with those from VERITAS [107] (dash dotted lines), MAGIC [108] (dotted lines) and HAWC [109] (dashed lines) with corrected J-factors (see section 5 for details). We also include the thermal cross section (up to $m_\chi \sim 200$ TeV, red line) and the partial wave unitarity bound for nearby dSphs (grey dashed line) [16, 47].

cross section up to $m_\chi \sim 200$ TeV [16, 47] and the partial wave unitarity bound for point-like particle DM assuming the relative velocity $v_{\text{rel}} \sim 2 \times 10^{-5}$ in the dSphs [47].

Figure 5 displays the 95% CL lower limits on heavy DM lifetime (τ_χ). Similar to the annihilation case, the inclusion of the electromagnetic cascades significantly improves the constraints for heavy m_χ , particularly for the $\mu^+\mu^-$ channel starting from $m_\chi \sim 10^3$ GeV. Unlike the annihilation case, constraints on the lifetime τ are only mildly weakened with increasing m_χ from 10^3 GeV, as the decay rate is proportional to $1/m_\chi$. Synchrotron emission also tightens the constraints on τ for $m_\chi \gtrsim 10^7 - 10^9$ GeV.

We present a complete set of constraints on heavy DM annihilation cross section and decay lifetime in figure 6 and figure 7, respectively. These constraints encompass six annihilation/decay channels and are derived from 8 classical dSphs. Among these dSphs, Draco stands out as the most stringent individual constraint for both annihilation and decay cases due to its substantial J-factors. The structures in constraints for $m_\chi \gtrsim 10^7 - 10^9$ GeV, attributed to synchrotron emission, are a consistent feature across all dSphs and channels. This effect is more pronounced for channels involving leptons, such as $\mu^+\mu^-$ and $\tau^+\tau^-$. In addition to individual dSph constraints, we also include constraints derived from stacking all 8 dSphs, as described in the section 4. We observe slightly improved limits from stacking 8 dSphs compared to the strongest limits from individual dSphs. The stacking limits are most likely driven by Draco, which has the largest J-factors among the target dSphs.

As a baseline of the analysis, we have assumed that dSphs are extended sources, and their DM halos follow the NFW density profile with truncation. A recent study [110] investigated the impact of considering the extension of dSphs when searching for DM signals with *Fermi*-LAT. They found that modeling dSphs as extended sources weakened the annihilation constraints by a factor of approximately 2, depending on the specific dSph and channel under

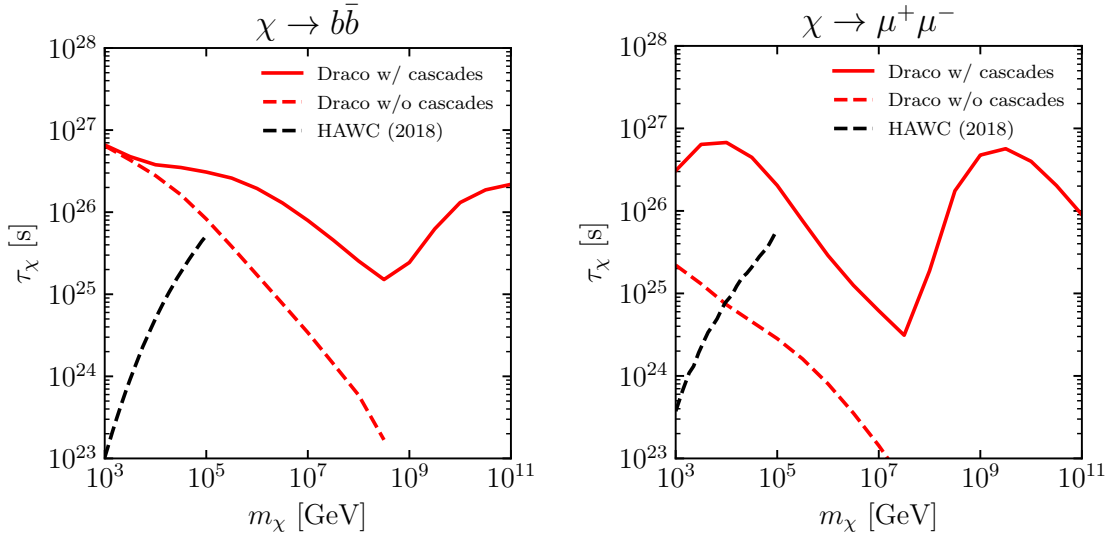


Figure 5. 95% CL lower limits on the lifetime τ_χ for the $b\bar{b}$ (left panel) and $\mu^+\mu^-$ (right panel) channel from Draco. Constraints with (solid red lines) and without (dashed red lines) electromagnetic cascades are included.

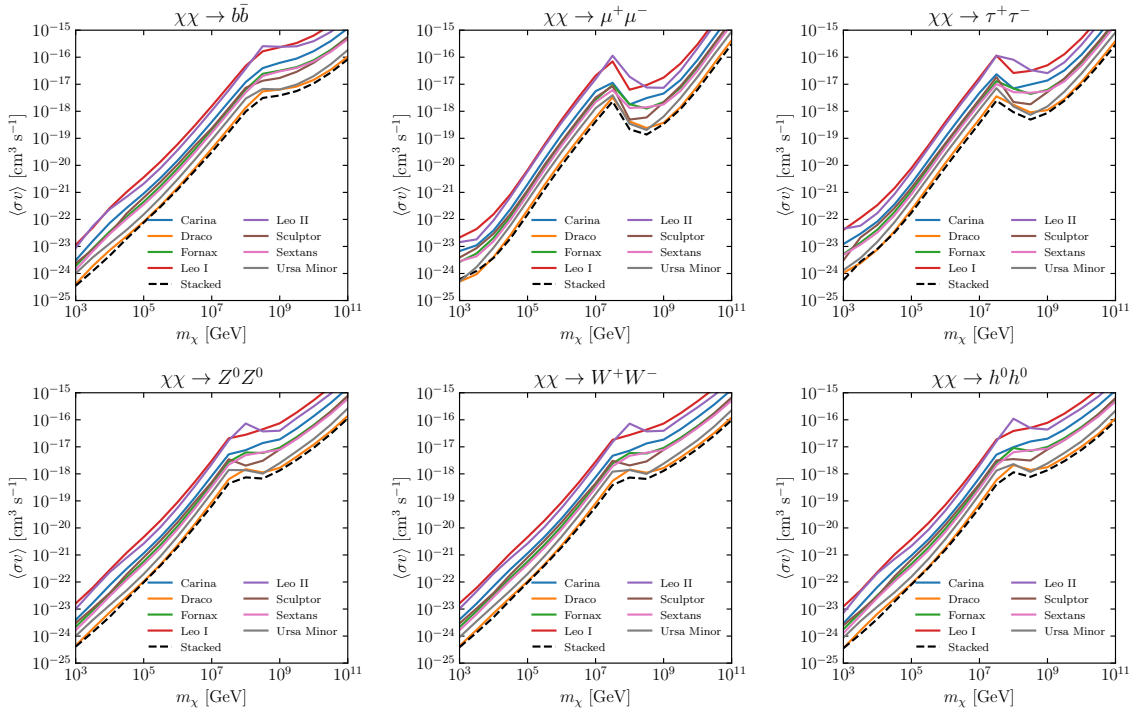


Figure 6. 95% CL upper limits on the annihilation cross section $\langle\sigma v\rangle$ for 6 channels and 8 dSphs. We also include the limits from stacking 8 dSphs (dashed lines).

consideration. To explore this effect, we treat the dSphs as point sources and repeat the data analysis for the $b\bar{b}$ channel. We make the assumption that the J-factors of the dSphs in the point-source approximation are equal to the $J^{\text{ann}}(\theta_\Delta)$ and $J^{\text{dec}}(\theta_\Delta)$ as presented in Table 2

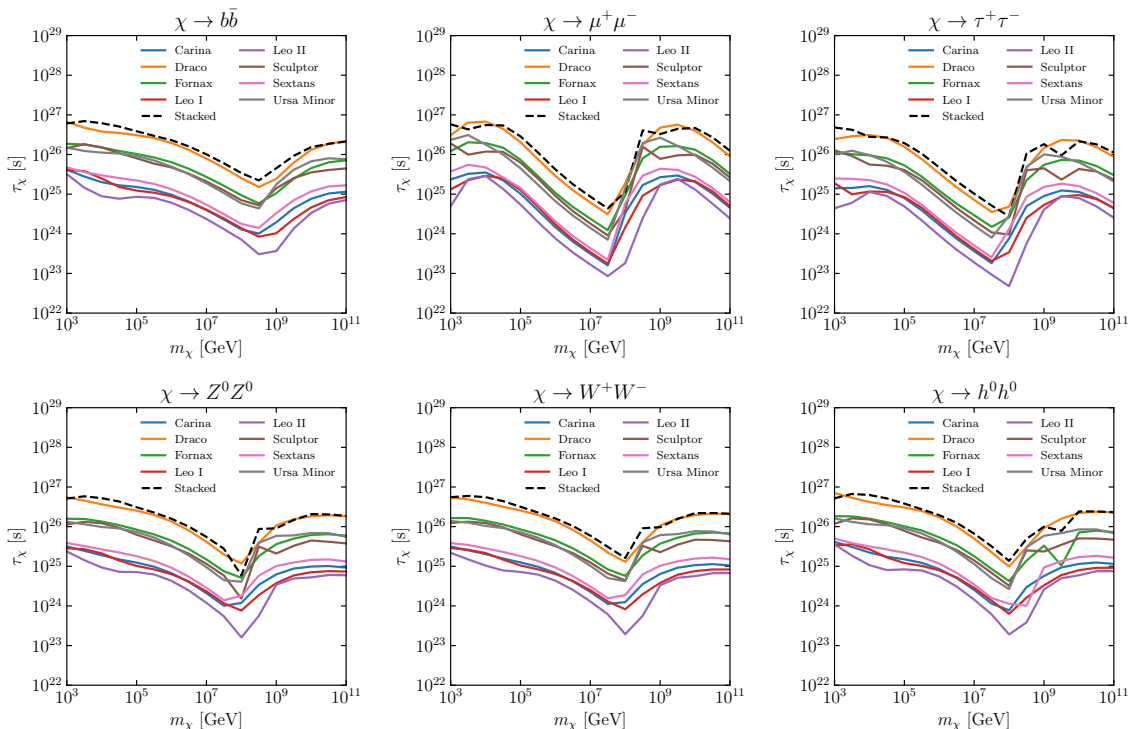


Figure 7. 95% CL lower limits on the lifetime τ_χ for 6 channels and 8 dSphs. We also include the limits from stacking 8 dSphs (dashed lines).

for the extended cases, which corresponds to an aggressive assumption for the point-source hypothesis. Figure 8 shows the ratios of the constraints on $\langle\sigma v\rangle$ (left panel) and $1/\tau_\chi$ (right panel) between the extended and point-source analyses for the $b\bar{b}$ channel. We observe that the constraints are generally weakened in the extended analysis. The ratios for the annihilation $\langle\sigma v\rangle$ vary from approximately 1 to 2, depending on the target dSph and mass m_χ . The range of ratios for $1/\tau_\chi$ is more variable, ranging from around 1 to nearly 9. The weakening effect is more pronounced for DM decay since the extended signal for DM decay is less concentrated at the center of the dSphs, as demonstrated in the 2D templates in Appendix A. Our results are qualitatively consistent with the findings of Ref. [110].

Finally, we investigate the impact of varying magnetic fields in the dSphs. The magnetic field strength could alter the results since the dominant secondary process in the *Fermi* energy range is affected by the energy partition between the background magnetic field and photon field. Ref. [111] has shown that the magnetic field in dSphs are usually less than a few μG and can reach values as high as $\sim 10 \mu\text{G}$. In our fiducial model, we assume a magnetic field strength of $B = 1 \mu\text{G}$. The energy density of the magnetic field strength in this range is similar to that of the CMB [112]. Varying magnetic field in this range is important as the energy losses of the inverse-Compton and synchrotron processes are comparable. Therefore, we test $B = 10 \mu\text{G}$ to reflect an extreme case and consider systematics coming from the magnetic field variation within a galaxy. Figure 9 displays the expected gamma-ray spectra at Earth for the $b\bar{b}$ channel in the left panel and the $\mu^+\mu^-$ channel in the right panel for three DM masses, similar to figure 3. The solid lines correspond to $B = 1 \mu\text{G}$, the fiducial

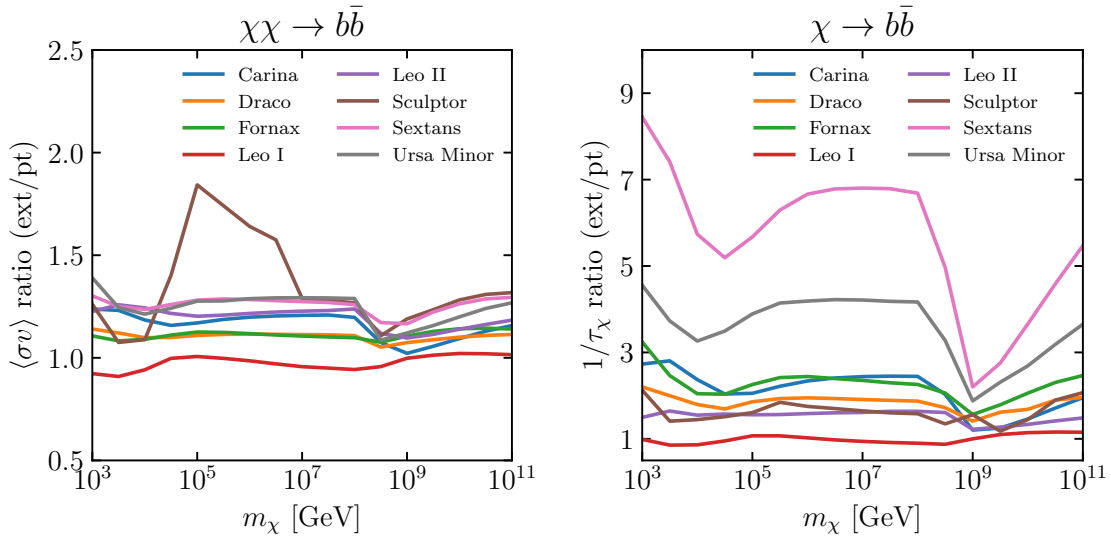


Figure 8. Ratios of the constraints on $\langle\sigma v\rangle$ (left panel) and $1/\tau_\chi$ (right panel) between the extended and point-source analysis. The annihilation/decay channel is $b\bar{b}$ and 8 dSphs are included.

value for the main results, while the dash-dotted lines represent an alternative magnetic field strength of $B = 10 \mu\text{G}$. Figure 10 compares the constraints on $\langle\sigma v\rangle$ between $B = 1 \mu\text{G}$ and $B = 10 \mu\text{G}$ for the $b\bar{b}$ (left panel) and $\mu^+\mu^-$ (right panel) channels. Generally, an increase in the magnetic field reduces the inverse-Compton emission and increases the synchrotron emission. Therefore, constraints with $B = 10 \mu\text{G}$ are weaker than those with $B = 1 \mu\text{G}$ for $m_\chi \lesssim 10^7 - 10^8 \text{ GeV}$ in which the inverse-Compton emission is more important than the synchrotron emission in the LAT energy range, and vice versa. In most cases, the constraints change by less than one order of magnitude, depending on m_χ . In figure 11, we make the same comparison for constraints on τ_χ . Once again, changing B from $1 \mu\text{G}$ to $10 \mu\text{G}$ alters the constraints by at most one order of magnitude.

6 Summary

We used 14 years of *Fermi*-LAT data to search for gamma-ray signals from heavy DM with $m_\chi \gtrsim 10^3 \text{ GeV}$ in 8 classical dSphs, and constrained the annihilation cross section and decay lifetime. In particular, we incorporated the effects of electromagnetic cascades to better probe DM heavier than 1 TeV together with the spatial extension of target dSphs considering their cosmological evolution under the gravitational potential of the Milky Way. We also quantified the impacts of the spatial extension and the magnetic field strength, and found that resulting systematic uncertainties are less than one order of magnitude. We showed that our dSph constraints from the LAT non-detection of gamma-ray signals with electromagnetic cascades surpass not only those without cascades but also the limits derived from very high-energy gamma-ray facilities such as VERITAS, MAGIC and HAWC. Our findings offer valuable complementary constraints on heavy DM, in conjunction with observations of high-energy gamma rays (e.g., from galaxy clusters [33, 39] and the Milky Way halo [44]), cosmic rays [69, 71], and neutrinos [20, 73].

We demonstrated that incorporating the electromagnetic cascades reinforces the dSph search for heavy DM by *Fermi*-LAT. Future observations of gamma rays and neutrinos will

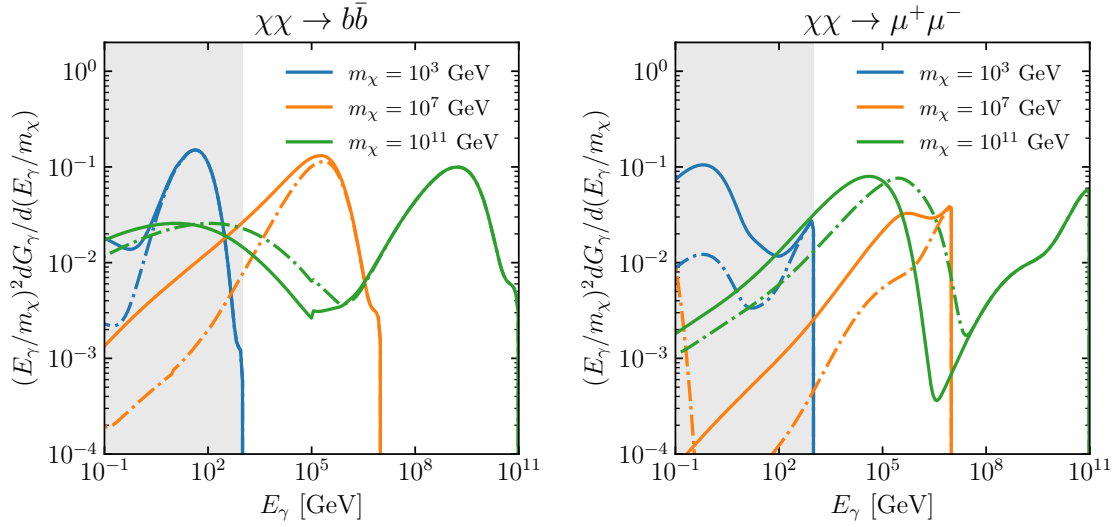


Figure 9. Gamma-ray spectra from DM annihilation with 3 different masses: $m_\chi = 10^3$ GeV (blue), 10^7 GeV (orange), and 10^{11} GeV (green). The solid lines consider $B = 1 \mu\text{G}$, the fiducial value for the main results. The dash-dotted lines consider an alternative magnetic field strength with $B = 10 \mu\text{G}$.

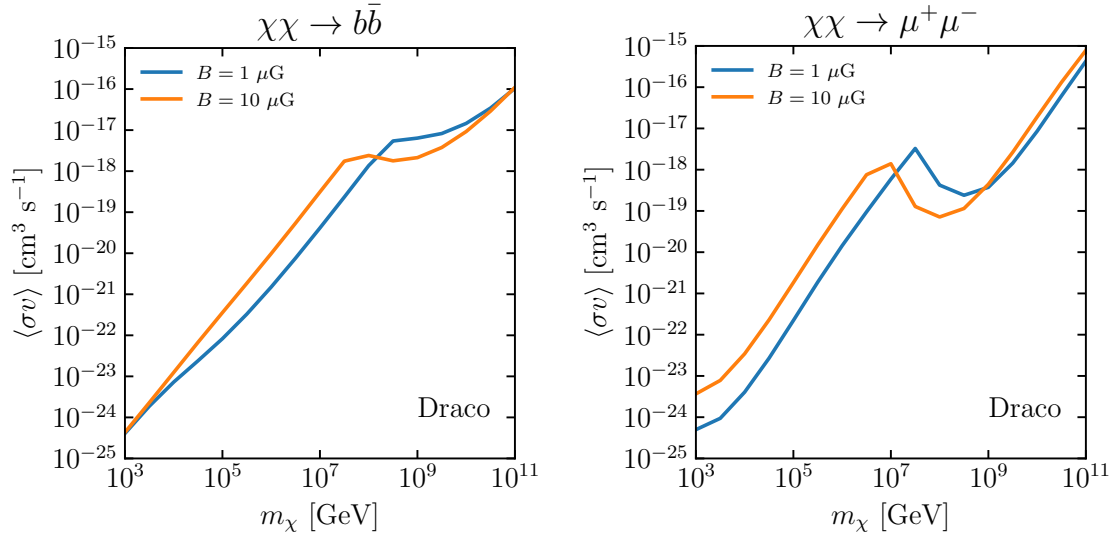


Figure 10. Constraints on $\langle\sigma v\rangle$ for the $b\bar{b}$ (left panel) and $\mu^+\mu^-$ (right panel) channels using Draco as dSph target. The plots show the comparison between $B = 1 \mu\text{G}$ and $B = 10 \mu\text{G}$ respectively in blue and orange.

also benefit from accounting for such effects [113]. Meanwhile, it is crucial to consider the cosmological evolution of dSphs in the Milky Way to accurately estimate their J-factors and spatial extensions, which will enable us to establish more reliable constraints [114] or possibly even detection [115] in the future.

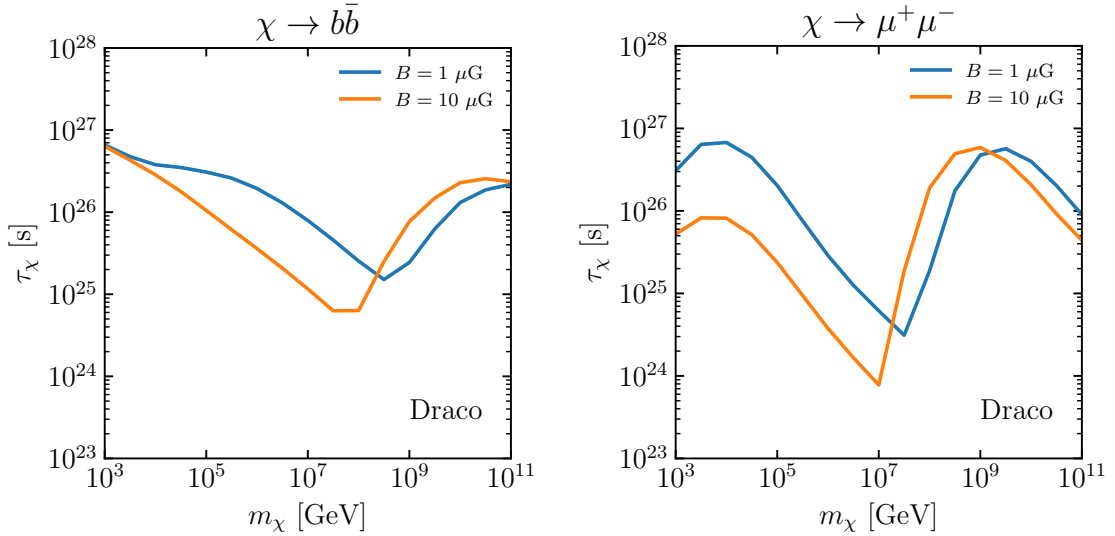


Figure 11. Constraints on τ_χ for the $b\bar{b}$ (left panel) and $\mu^+\mu^-$ (right panel) channels using Draco as dSph target. The plots show the comparison between $B = 1 \mu\text{G}$ and $B = 10 \mu\text{G}$ respectively in blue and orange.

Acknowledgments

The *Fermi* LAT Collaboration acknowledges generous ongoing support from a number of agencies and institutes that have supported both the development and the operation of the LAT as well as scientific data analysis. These include the National Aeronautics and Space Administration and the Department of Energy in the United States, the Commissariat à l’Energie Atomique and the Centre National de la Recherche Scientifique / Institut National de Physique Nucléaire et de Physique des Particules in France, the Agenzia Spaziale Italiana and the Istituto Nazionale di Fisica Nucleare in Italy, the Ministry of Education, Culture, Sports, Science and Technology (MEXT), High Energy Accelerator Research Organization (KEK) and Japan Aerospace Exploration Agency (JAXA) in Japan, and the K. A. Wallenberg Foundation, the Swedish Research Council and the Swedish National Space Board in Sweden.

Additional support for science analysis during the operations phase is gratefully acknowledged from the Istituto Nazionale di Astrofisica in Italy and the Centre National d’Études Spatiales in France. This work performed in part under DOE Contract DE-AC02-76SF00515.

The authors express our gratitude to Soheila Abdollahi, Regina Caputo, Milena Crnogorčević, and Davide Serini for their valuable assistance in preparing the draft. We especially thank Davide Serini, Regina Caputo, and Donggeun Tak for providing insightful comments on the draft. We also thank Shin’icuro Ando for sharing the codes on the DM template model for the dwarf satellites. D.S., N.H., and K.M. are supported by JSPS KAKENHI Grant Number 20H05852. The work of N.H. is also supported in part by the Scientific Research 22K14035 MEXT Leading Initiative for Excellent Young Researchers Grant Number 2023L0013. The work of K.M. was also supported by the NSF Grants No. AST-2108466 and No. AST-2108467, and KAKENHI No. 20H01901.

Note added. While we are finalizing this paper, Ref. [116] of a close research interest appeared. The major difference is the treatment of the source extension. Also, the model for

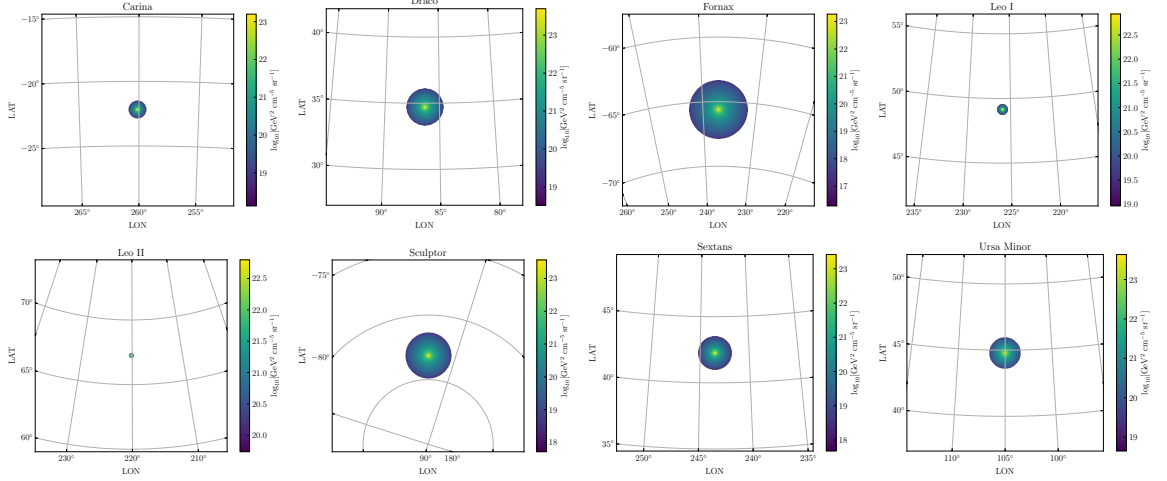


Figure 12. $\frac{dJ^{\text{ann}}}{d\Omega}(\Omega)$ for 8 dSphs.

the diffusion is different from each other.

A Spatial templates

In our data analysis, we model dSphs as extended sources. The spatial template is determined by median values of ρ_s and r_s as described in section 2. We use the CLUMPY package to calculate the differential J-factors $\frac{dJ^{\text{ann}}}{d\Omega}(\Omega)$ and $\frac{dJ^{\text{dec}}}{d\Omega}(\Omega)$ over the ROIs of dSphs.

Figure 12 shows the templates for $\frac{dJ^{\text{ann}}}{d\Omega}(\Omega)$ for 8 target dSphs, before they are convolved with the *Fermi*-LAT PSF. We calculate $\frac{dJ^{\text{ann}}}{d\Omega}(\Omega)$ up to the θ_Δ for each dSph (see Table 2), while figure 13 shows the templates for $\frac{dJ^{\text{dec}}}{d\Omega}(\Omega)$. In the case of annihilation, the DM signals are highly concentrated at the centers of the dSphs. However, in the case of decay, the DM signals are less concentrated and more diffuse, evenly distributed.

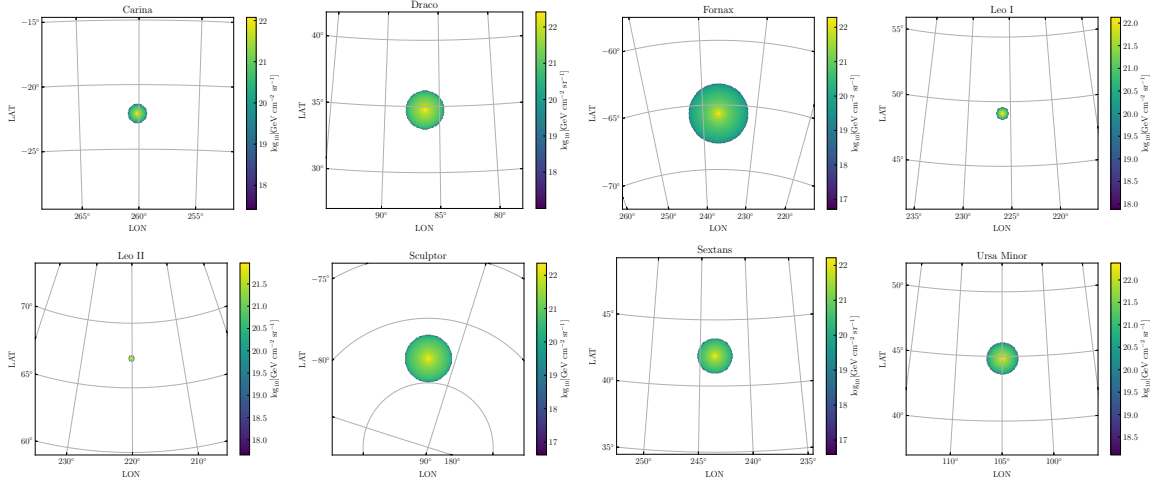


Figure 13. $\frac{dJ^{\text{dec}}}{d\Omega}(\Omega)$ for 8 dSphs.

References

- [1] PLANCK collaboration, *Planck 2018 results. VI. Cosmological parameters*, *Astron. Astrophys.* **641** (2020) A6 [[1807.06209](#)].
- [2] PLANCK collaboration, *Planck 2018 results. X. Constraints on inflation*, *Astron. Astrophys.* **641** (2020) A10 [[1807.06211](#)].
- [3] G. Bertone and D. Hooper, *History of dark matter*, *Rev. Mod. Phys.* **90** (2018) 045002 [[1605.04909](#)].
- [4] T. Lin, *Dark matter models and direct detection*, *PoS* **333** (2019) 009 [[1904.07915](#)].
- [5] B.R. Safdi, *TASI Lectures on the Particle Physics and Astrophysics of Dark Matter*, **2303.02169**.
- [6] S. Hoof, A. Geringer-Sameth and R. Trotta, *A Global Analysis of Dark Matter Signals from 27 Dwarf Spheroidal Galaxies using 11 Years of Fermi-LAT Observations*, *JCAP* **02** (2020) 012 [[1812.06986](#)].
- [7] GAMBIT collaboration, *Thermal WIMPs and the scale of new physics: global fits of Dirac dark matter effective field theories*, *Eur. Phys. J. C* **81** (2021) 992 [[2106.02056](#)].
- [8] M. Srednicki, R. Watkins and K.A. Olive, *Calculations of Relic Densities in the Early Universe*, *Nucl. Phys. B* **310** (1988) 693.
- [9] V.K. Dubrovich, D. Fargion and M.Y. Khlopov, *Primordial bound systems of superheavy particles as the source of ultrahigh-energy cosmic rays*, *Astropart. Phys.* **22** (2004) 183 [[hep-ph/0312105](#)].
- [10] J. Hisano, S. Matsumoto, M. Nagai, O. Saito and M. Senami, *Non-perturbative effect on thermal relic abundance of dark matter*, *Phys. Lett. B* **646** (2007) 34 [[hep-ph/0610249](#)].
- [11] G. Steigman, B. Dasgupta and J.F. Beacom, *Precise Relic WIMP Abundance and its Impact on Searches for Dark Matter Annihilation*, *Phys. Rev. D* **86** (2012) 023506 [[1204.3622](#)].
- [12] B. von Harling and K. Petraki, *Bound-state formation for thermal relic dark matter and unitarity*, *JCAP* **12** (2014) 033 [[1407.7874](#)].
- [13] J. Bramante and J. Unwin, *Superheavy Thermal Dark Matter and Primordial Asymmetries*, *JHEP* **02** (2017) 119 [[1701.05859](#)].
- [14] I. Baldes and K. Petraki, *Asymmetric thermal-relic dark matter: Sommerfeld-enhanced freeze-out, annihilation signals and unitarity bounds*, *JCAP* **09** (2017) 028 [[1703.00478](#)].
- [15] M. Cirelli, Y. Gouttenoire, K. Petraki and F. Sala, *Homeopathic Dark Matter, or how diluted heavy substances produce high energy cosmic rays*, *JCAP* **02** (2019) 014 [[1811.03608](#)].
- [16] J. Smirnov and J.F. Beacom, *TeV-Scale Thermal WIMPs: Unitarity and its Consequences*, *Phys. Rev. D* **100** (2019) 043029 [[1904.11503](#)].
- [17] D. Bhatia and S. Mukhopadhyay, *Unitarity limits on thermal dark matter in (non-)standard cosmologies*, *JHEP* **03** (2021) 133 [[2010.09762](#)].
- [18] I. Baldes, Y. Gouttenoire, F. Sala and G. Servant, *Supercool composite Dark Matter beyond 100 TeV*, *JHEP* **07** (2022) 084 [[2110.13926](#)].
- [19] K.N. Abazajian, S. Blanchet and J.P. Harding, *Current and Future Constraints on Dark Matter from Prompt and Inverse-Compton Photon Emission in the Isotropic Diffuse Gamma-ray Background*, *Phys. Rev. D* **85** (2012) 043509 [[1011.5090](#)].
- [20] K. Murase and J.F. Beacom, *Constraining Very Heavy Dark Matter Using Diffuse Backgrounds of Neutrinos and Cascaded Gamma Rays*, *JCAP* **10** (2012) 043 [[1206.2595](#)].

- [21] T. Bringmann, F. Calore, M. Di Mauro and F. Donato, *Constraining dark matter annihilation with the isotropic γ -ray background: updated limits and future potential*, *Phys. Rev. D* **89** (2014) 023012 [[1303.3284](#)].
- [22] M. Ajello et al., *The Origin of the Extragalactic Gamma-Ray Background and Implications for Dark-Matter Annihilation*, *Astrophys. J. Lett.* **800** (2015) L27 [[1501.05301](#)].
- [23] FERMI-LAT collaboration, *Limits on Dark Matter Annihilation Signals from the Fermi LAT 4-year Measurement of the Isotropic Gamma-Ray Background*, *JCAP* **09** (2015) 008 [[1501.05464](#)].
- [24] M. Di Mauro, *Isotropic diffuse gamma-ray background: unveiling Dark Matter components beyond the contribution of astrophysical sources*, in *5th International Fermi Symposium*, 2, 2015 [[1502.02566](#)].
- [25] M. Di Mauro and F. Donato, *Composition of the Fermi-LAT isotropic gamma-ray background intensity: Emission from extragalactic point sources and dark matter annihilations*, *Phys. Rev. D* **91** (2015) 123001 [[1501.05316](#)].
- [26] W. Liu, X.-J. Bi, S.-J. Lin and P.-F. Yin, *Constraints on dark matter annihilation and decay from the isotropic gamma-ray background*, *Chin. Phys. C* **41** (2017) 045104 [[1602.01012](#)].
- [27] C. Blanco and D. Hooper, *Constraints on Decaying Dark Matter from the Isotropic Gamma-Ray Background*, *JCAP* **03** (2019) 019 [[1811.05988](#)].
- [28] M. Ackermann, M. Ajello, A. Allafort, L. Baldini, J. Ballet, G. Barbiellini et al., *Constraints on dark matter annihilation in clusters of galaxies with the Fermi large area telescope*, *J. Cosmology Astropart. Phys.* **2010** (2010) 025 [[1002.2239](#)].
- [29] X. Huang, G. Vertongen and C. Weniger, *Probing Dark Matter Decay and Annihilation with Fermi LAT Observations of Nearby Galaxy Clusters*, *JCAP* **01** (2012) 042 [[1110.1529](#)].
- [30] A. Pinzke, C. Pfrommer and L. Bergström, *Prospects of detecting gamma-ray emission from galaxy clusters: Cosmic rays and dark matter annihilations*, *Phys. Rev. D* **84** (2011) 123509 [[1105.3240](#)].
- [31] A. Abramowski, F. Acero, F. Aharonian, A.G. Akhperjanian, G. Anton, A. Balzer et al., *Search for Dark Matter Annihilation Signals from the Fornax Galaxy Cluster with H.E.S.S.*, *Astrophys. J.* **750** (2012) 123 [[1202.5494](#)].
- [32] S. Ando and D. Nagai, *Fermi-LAT constraints on dark matter annihilation cross section from observations of the Fornax cluster*, *J. Cosmology Astropart. Phys.* **2012** (2012) 017 [[1201.0753](#)].
- [33] K. Murase and J.F. Beacom, *Galaxy Clusters as Reservoirs of Heavy Dark Matter and High-Energy Cosmic Rays: Constraints from Neutrino Observations*, *JCAP* **02** (2013) 028 [[1209.0225](#)].
- [34] O. Urban, N. Werner, S.W. Allen, A. Simionescu, J.S. Kaastra and L.E. Strigari, *A Suzaku Search for Dark Matter Emission Lines in the X-ray Brightest Galaxy Clusters*, *Mon. Not. Roy. Astron. Soc.* **451** (2015) 2447 [[1411.0050](#)].
- [35] FERMI-LAT collaboration, *Search for extended gamma-ray emission from the Virgo galaxy cluster with Fermi-LAT*, *Astrophys. J.* **812** (2015) 159 [[1510.00004](#)].
- [36] X. Tan, M. Colavincenzo and S. Ammazzalorso, *Bounds on WIMP dark matter from galaxy clusters at low redshift*, *Mon. Not. Roy. Astron. Soc.* **495** (2020) 114 [[1907.06905](#)].
- [37] C. Thorpe-Morgan, D. Malyshev, C.-A. Stegen, A. Santangelo and J. Jochum, *Annihilating dark matter search with 12 yr of Fermi LAT data in nearby galaxy clusters*, *Mon. Not. Roy. Astron. Soc.* **502** (2021) 4039 [[2010.11006](#)].

- [38] M. Di Mauro, J. Pérez-Romero, M.A. Sánchez-Conde and N. Fornengo, *Constraining the dark matter contribution of γ rays in clusters of galaxies using Fermi-LAT data*, *Phys. Rev. D* **107** (2023) 083030 [[2303.16930](#)].
- [39] D. Song, K. Murase and A. Kheirandish, *Constraining decaying very heavy dark matter from galaxy clusters with 14 year Fermi-LAT data*, [2308.00589](#).
- [40] L. Bergstrom, P. Ullio and J.H. Buckley, *Observability of gamma-rays from dark matter neutralino annihilations in the Milky Way halo*, *Astropart. Phys.* **9** (1998) 137 [[astro-ph/9712318](#)].
- [41] Y. Ascasibar, P. Jean, C. Boehm and J. Knoedlseder, *Constraints on dark matter and the shape of the Milky Way dark halo from the 511-keV line*, *Mon. Not. Roy. Astron. Soc.* **368** (2006) 1695 [[astro-ph/0507142](#)].
- [42] M. Kamionkowski, S.M. Koushiappas and M. Kuhlen, *Galactic substructure and dark-matter annihilation in the Milky Way halo*, *Phys. Rev. D* **81** (2010) 043532 [[1001.3144](#)].
- [43] K. Murase, R. Laha, S. Ando and M. Ahlers, *Testing the Dark Matter Scenario for PeV Neutrinos Observed in IceCube*, *Phys. Rev. Lett.* **115** (2015) 071301 [[1503.04663](#)].
- [44] T. Cohen, K. Murase, N.L. Rodd, B.R. Safdi and Y. Soreq, *γ -ray Constraints on Decaying Dark Matter and Implications for IceCube*, *Phys. Rev. Lett.* **119** (2017) 021102 [[1612.05638](#)].
- [45] L.J. Chang, M. Lisanti and S. Mishra-Sharma, *Search for dark matter annihilation in the Milky Way halo*, *Phys. Rev. D* **98** (2018) 123004 [[1804.04132](#)].
- [46] T.N. Maity, A.K. Saha, A. Dubey and R. Laha, *Search for dark matter using sub-PeV γ -rays observed by Tibet AS γ* , [2105.05680](#).
- [47] D. Tak, M. Baumgart, N.L. Rodd and E. Pueschel, *Current and Future γ -Ray Searches for Dark Matter Annihilation Beyond the Unitarity Limit*, *Astrophys. J. Lett.* **938** (2022) L4 [[2208.11740](#)].
- [48] F. Stoehr, S.D.M. White, V. Springel, G. Tormen and N. Yoshida, *Dark matter annihilation in the halo of the Milky Way*, *Mon. Not. Roy. Astron. Soc.* **345** (2003) 1313 [[astro-ph/0307026](#)].
- [49] J. Diemand, M. Kuhlen and P. Madau, *Dark matter substructure and gamma-ray annihilation in the Milky Way halo*, *Astrophys. J.* **657** (2007) 262 [[astro-ph/0611370](#)].
- [50] I. Cholis and P. Salucci, *Extracting limits on Dark Matter annihilation from gamma-ray observations towards dwarf spheroidal galaxies*, *Phys. Rev. D* **86** (2012) 023528 [[1203.2954](#)].
- [51] E. Carlson, D. Hooper and T. Linden, *Improving the Sensitivity of Gamma-Ray Telescopes to Dark Matter Annihilation in Dwarf Spheroidal Galaxies*, *Phys. Rev. D* **91** (2015) 061302 [[1409.1572](#)].
- [52] A. Lopez, C. Savage, D. Spolyar and D.Q. Adams, *Fermi/LAT observations of Dwarf Galaxies highly constrain a Dark Matter Interpretation of Excess Positrons seen in AMS-02, HEAT, and PAMELA*, *JCAP* **03** (2016) 033 [[1501.01618](#)].
- [53] FERMI-LAT collaboration, *Searching for Dark Matter Annihilation from Milky Way Dwarf Spheroidal Galaxies with Six Years of Fermi Large Area Telescope Data*, *Phys. Rev. Lett.* **115** (2015) 231301 [[1503.02641](#)].
- [54] V. Bonnivard et al., *Dark matter annihilation and decay in dwarf spheroidal galaxies: The classical and ultrafaint dSphs*, *Mon. Not. Roy. Astron. Soc.* **453** (2015) 849 [[1504.02048](#)].
- [55] M.G. Baring, T. Ghosh, F.S. Queiroz and K. Sinha, *New Limits on the Dark Matter Lifetime from Dwarf Spheroidal Galaxies using Fermi-LAT*, *Phys. Rev. D* **93** (2016) 103009 [[1510.00389](#)].

- [56] MAGIC, FERMI-LAT collaboration, *Limits to Dark Matter Annihilation Cross-Section from a Combined Analysis of MAGIC and Fermi-LAT Observations of Dwarf Satellite Galaxies*, *JCAP* **02** (2016) 039 [[1601.06590](#)].
- [57] F. Calore, P.D. Serpico and B. Zaldívar, *Dark matter constraints from dwarf galaxies: a data-driven analysis*, *JCAP* **10** (2018) 029 [[1803.05508](#)].
- [58] S. Ando et al., *Discovery prospects of dwarf spheroidal galaxies for indirect dark matter searches*, *JCAP* **10** (2019) 040 [[1905.07128](#)].
- [59] A. Kar, S. Mitra, B. Mukhopadhyaya and T.R. Choudhury, *Heavy dark matter particle annihilation in dwarf spheroidal galaxies: radio signals at the SKA telescope*, *Phys. Rev. D* **101** (2020) 023015 [[1905.11426](#)].
- [60] A. Alvarez, F. Calore, A. Genina, J. Read, P.D. Serpico and B. Zaldívar, *Dark matter constraints from dwarf galaxies with data-driven J-factors*, *JCAP* **09** (2020) 004 [[2002.01229](#)].
- [61] FERMI-LAT collaboration, *Dark Matter search in dwarf irregular galaxies with the Fermi Large Area Telescope*, *PoS ICRC2021* (2021) 509 [[2109.11291](#)].
- [62] S. Ando et al., *Decaying dark matter in dwarf spheroidal galaxies: Prospects for x-ray and gamma-ray telescopes*, *Phys. Rev. D* **104** (2021) 023022 [[2103.13242](#)].
- [63] S. Yoshida, G. Sigl and S.-j. Lee, *Extremely high-energy neutrinos, neutrino hot dark matter, and the highest energy cosmic rays*, *Phys. Rev. Lett.* **81** (1998) 5505 [[hep-ph/9808324](#)].
- [64] P. Blasi and R.K. Sheth, *Halo dark matter and ultrahigh-energy cosmic rays*, *Phys. Lett. B* **486** (2000) 233 [[astro-ph/0006316](#)].
- [65] L. Marzola and F.R. Urban, *Ultra High Energy Cosmic Rays & Super-heavy Dark Matter*, *Astropart. Phys.* **93** (2017) 56 [[1611.07180](#)].
- [66] A. Cuoco, J. Heisig, M. Korsmeier and M. Krämer, *Constraining heavy dark matter with cosmic-ray antiprotons*, *JCAP* **04** (2018) 004 [[1711.05274](#)].
- [67] A.D. Supanitsky and G. Medina-Tanco, *Ultra high energy cosmic rays from super-heavy dark matter in the context of large exposure observatories*, *JCAP* **11** (2019) 036 [[1909.09191](#)].
- [68] E. Alcantara, L.A. Anchordoqui and J.F. Soriano, *Hunting for superheavy dark matter with the highest-energy cosmic rays*, *Phys. Rev. D* **99** (2019) 103016 [[1903.05429](#)].
- [69] K. Ishiwata, O. Macias, S. Ando and M. Arimoto, *Probing heavy dark matter decays with multi-messenger astrophysical data*, *JCAP* **01** (2020) 003 [[1907.11671](#)].
- [70] H. Motz, *Constraints on heavy dark matter annihilation and decay from electron and positron cosmic ray spectra*, *SciPost Phys. Proc.* **12** (2023) 035.
- [71] S. Das, K. Murase and T. Fujii, *Revisiting ultrahigh-energy constraints on decaying superheavy dark matter*, *Phys. Rev. D* **107** (2023) 103013 [[2302.02993](#)].
- [72] ICECUBE collaboration, *IceCube Search for Dark Matter Annihilation in nearby Galaxies and Galaxy Clusters*, *Phys. Rev. D* **88** (2013) 122001 [[1307.3473](#)].
- [73] M. Chianese, D.F.G. Fiorillo, R. Hajjar, G. Miele, S. Morisi and N. Saviano, *Heavy decaying dark matter at future neutrino radio telescopes*, *JCAP* **05** (2021) 074 [[2103.03254](#)].
- [74] D.F.G. Fiorillo, V.B. Valera, M. Bustamante and W. Winter, *Searches for dark matter decay with ultra-high-energy neutrinos endure backgrounds*, [2307.02538](#).
- [75] T.R. Slatyer, N. Padmanabhan and D.P. Finkbeiner, *CMB Constraints on WIMP Annihilation: Energy Absorption During the Recombination Epoch*, *Phys. Rev. D* **80** (2009) 043526 [[0906.1197](#)].
- [76] M. Kawasaki, H. Nakatsuka, K. Nakayama and T. Sekiguchi, *Revisiting CMB constraints on dark matter annihilation*, *JCAP* **12** (2021) 015 [[2105.08334](#)].

- [77] S. Ando, A. Geringer-Sameth, N. Hiroshima, S. Hoof, R. Trotta and M.G. Walker, *Structure formation models weaken limits on WIMP dark matter from dwarf spheroidal galaxies*, *Phys. Rev. D* **102** (2020) 061302 [[2002.11956](#)].
- [78] G.D. Martinez, *A robust determination of Milky Way satellite properties using hierarchical mass modelling*, *Mon. Not. Roy. Astron. Soc.* **451** (2015) 2524 [[1309.2641](#)].
- [79] A. Geringer-Sameth, S.M. Koushiappas and M. Walker, *Dwarf galaxy annihilation and decay emission profiles for dark matter experiments*, *Astrophys. J.* **801** (2015) 74 [[1408.0002](#)].
- [80] K. Hayashi, K. Ichikawa, S. Matsumoto, M. Ibe, M.N. Ishigaki and H. Sugai, *Dark matter annihilation and decay from non-spherical dark halos in galactic dwarf satellites*, *Mon. Not. Roy. Astron. Soc.* **461** (2016) 2914 [[1603.08046](#)].
- [81] A.B. Pace and L.E. Strigari, *Scaling Relations for Dark Matter Annihilation and Decay Profiles in Dwarf Spheroidal Galaxies*, *Mon. Not. Roy. Astron. Soc.* **482** (2019) 3480 [[1802.06811](#)].
- [82] J.F. Navarro, C.S. Frenk and S.D.M. White, *A Universal density profile from hierarchical clustering*, *Astrophys. J.* **490** (1997) 493 [[astro-ph/9611107](#)].
- [83] M.G. Walker, M. Mateo, E.W. Olszewski, B. Sen and M. Woodroffe, *Clean Kinematic Samples in Dwarf Spheroidals: An Algorithm for Evaluating Membership and Estimating Distribution Parameters When Contamination is Present*, *Astron. J.* **137** (2009) 3109 [[0811.1990](#)].
- [84] M.G. Walker, E.W. Olszewski and M. Mateo, *Bayesian analysis of resolved stellar spectra: application to MMT/Hectochelle observations of the Draco dwarf spheroidal*, *Mon. Not. Roy. Astron. Soc.* **448** (2015) 2717 [[1503.02589](#)].
- [85] M.G. Walker, M. Mateo, E.W. Olszewski, J. Penarrubia, N.W. Evans and G. Gilmore, *A Universal Mass Profile for Dwarf Spheroidal Galaxies*, *Astrophys. J.* **704** (2009) 1274 [[0906.0341](#)].
- [86] M. Mateo, E.W. Olszewski and M.G. Walker, *The Velocity Dispersion Profile of the Remote Dwarf Spheroidal Galaxy Leo. 1. A Tidal Hit and Run?*, *Astrophys. J.* **675** (2008) 201 [[0708.1327](#)].
- [87] M.E. Spencer, M. Mateo, M.G. Walker and E.W. Olszewski, *A Multi-epoch Kinematic Study of the Remote Dwarf Spheroidal Galaxy Leo II*, *Astrophys. J.* **836** (2017) 202 [[1702.08836](#)].
- [88] M. Mateo, N. Mirabal, A. Udalski, M. Szymanski, J. Kaluzny, M. Kubiak et al., *Discovery of a Tidal Extension of the Sagittarius Dwarf Spheroidal Galaxy*, *Astrophys. J. Lett.* **458** (1996) L13.
- [89] N. Hiroshima, S. Ando and T. Ishiyama, *Modeling evolution of dark matter substructure and annihilation boost*, *Phys. Rev. D* **97** (2018) 123002 [[1803.07691](#)].
- [90] X. Yang, H.J. Mo, Y. Zhang and F.C.v.d. Bosch, *An analytical model for the accretion of dark matter subhalos*, *Astrophys. J.* **741** (2011) 13 [[1104.1757](#)].
- [91] F. Jiang and F.C. van den Bosch, *Statistics of dark matter substructure – I. Model and universal fitting functions*, *Mon. Not. Roy. Astron. Soc.* **458** (2016) 2848 [[1403.6827](#)].
- [92] J. Penarrubia, A.J. Benson, M.G. Walker, G. Gilmore, A. McConnachie and L. Mayer, *The impact of dark matter cusps and cores on the satellite galaxy population around spiral galaxies*, *Mon. Not. Roy. Astron. Soc.* **406** (2010) 1290 [[1002.3376](#)].
- [93] A.S. Graus, J.S. Bullock, T. Kelley, M. Boylan-Kolchin, S. Garrison-Kimmel and Y. Qi, *How low does it go? Too few Galactic satellites with standard reionization quenching*, *Mon. Not. Roy. Astron. Soc.* **488** (2019) 4585 [[1808.03654](#)].

- [94] J.R. Hargis, B. Willman and A.H.G. Peter, *Too Many, Too Few, or Just Right? The Predicted Number and Distribution of Milky Way Dwarf Galaxies*, *Astrophys. J. Lett.* **795** (2014) L13 [[1407.4470](#)].
- [95] D. Foreman-Mackey, *corner.py: Scatterplot matrices in python*, *The Journal of Open Source Software* **1** (2016) 24.
- [96] C.W. Bauer, N.L. Rodd and B.R. Webber, *Dark matter spectra from the electroweak to the Planck scale*, *JHEP* **06** (2021) 121 [[2007.15001](#)].
- [97] T. Sjöstrand, S. Ask, J.R. Christiansen, R. Corke, N. Desai, P. Ilten et al., *An introduction to PYTHIA 8.2*, *Comput. Phys. Commun.* **191** (2015) 159 [[1410.3012](#)].
- [98] D.J. Fixsen, *The Temperature of the Cosmic Microwave Background*, *Astrophys. J.* **707** (2009) 916 [[0911.1955](#)].
- [99] Y.-T. Lin, J.J. Mohr and S.A. Stanford, *Near-IR properties of galaxy clusters: Luminosity as a binding mass predictor and the state of cluster baryons*, *Astrophys. J.* **591** (2003) 749 [[astro-ph/0304033](#)].
- [100] E.N. Kirby, J.G. Cohen, P. Guhathakurta, L. Cheng, J.S. Bullock and A. Gallazzi, *The Universal Stellar Mass-Stellar Metallicity Relation for Dwarf Galaxies*, *Astrophys. J.* **779** (2013) 102 [[1310.0814](#)].
- [101] T.M. Kneiske, T. Bretz, K. Mannheim and D.H. Hartmann, *Implications of cosmological gamma-ray absorption. 2. Modification of gamma-ray spectra*, *Astron. Astrophys.* **413** (2004) 807 [[astro-ph/0309141](#)].
- [102] M. Wood, R. Caputo, E. Charles, M. Di Mauro, J. Magill, J.S. Perkins et al., *Fermipy: An open-source Python package for analysis of Fermi-LAT Data*, in *35th International Cosmic Ray Conference (ICRC2017)*, vol. 301 of *International Cosmic Ray Conference*, p. 824, July, 2017, DOI [[1707.09551](#)].
- [103] A. Charbonnier, C. Combet and D. Maurin, *CLUMPY: a code for gamma-ray signals from dark matter structures*, *Comput. Phys. Commun.* **183** (2012) 656 [[1201.4728](#)].
- [104] V. Bonnivard, M. Hütten, E. Nezri, A. Charbonnier, C. Combet and D. Maurin, *CLUMPY : Jeans analysis, γ -ray and ν fluxes from dark matter (sub-)structures*, *Comput. Phys. Commun.* **200** (2016) 336 [[1506.07628](#)].
- [105] M. Hütten, C. Combet and D. Maurin, *CLUMPY v3: γ -ray and ν signals from dark matter at all scales*, *Comput. Phys. Commun.* **235** (2019) 336 [[1806.08639](#)].
- [106] W.A. Rolke, A.M. Lopez and J. Conrad, *Limits and confidence intervals in the presence of nuisance parameters*, *Nucl. Instrum. Meth. A* **551** (2005) 493 [[physics/0403059](#)].
- [107] A. Acharyya et al., *Search for Ultraheavy Dark Matter from Observations of Dwarf Spheroidal Galaxies with VERITAS*, *Astrophys. J.* **945** (2023) 101 [[2302.08784](#)].
- [108] MAGIC collaboration, *Combined searches for dark matter in dwarf spheroidal galaxies observed with the MAGIC telescopes, including new data from Coma Berenices and Draco*, *Phys. Dark Univ.* **35** (2022) 100912 [[2111.15009](#)].
- [109] HAWC collaboration, *Dark Matter Limits From Dwarf Spheroidal Galaxies with The HAWC Gamma-Ray Observatory*, *Astrophys. J.* **853** (2018) 154 [[1706.01277](#)].
- [110] M. Di Mauro, M. Stref and F. Calore, *Investigating the effect of Milky Way dwarf spheroidal galaxies extension on dark matter searches with Fermi-LAT data*, *Phys. Rev. D* **106** (2022) 123032 [[2212.06850](#)].
- [111] K.T. Chyży, M. Weźgowiec, R. Beck and D.J. Bomans, *Magnetic fields in Local Group dwarf irregulars*, *Astron. Astrophys.* **529** (2011) A94 [[1101.4647](#)].

- [112] K. Dolag, D. Grasso, V. Springel and I. Tkachev, *Constrained simulations of the magnetic field in the local Universe and the propagation of UHECRs*, *JCAP* **01** (2005) 009 [[astro-ph/0410419](#)].
- [113] D.M.H. Leung and K.C.Y. Ng, *Improving HAWC dark matter constraints with Inverse-Compton Emission*, [2312.08989](#).
- [114] M. Crnogorčević and T. Linden, *Strong Constraints on Dark Matter Annihilation in Ursa Major III/UNIONS 1*, [2311.14611](#).
- [115] A. McDaniel, M. Ajello, C.M. Karwin, M. Di Mauro, A. Drlica-Wagner and M. Sánchez-Conde, *Legacy Analysis of Dark Matter Annihilation from the Milky Way Dwarf Spheroidal Galaxies with 14 Years of Fermi-LAT Data*, [2311.04982](#).
- [116] X.-S. Hu, B.-Y. Zhu, T.-C. Liu and Y.-F. Liang, *Constraints on the annihilation of heavy dark matter in dwarf spheroidal galaxies with gamma-ray observations*, [2309.06151](#).